

\mathcal{U}^3 -xi: Pushing the Boundaries of Speaker Recognition via Incorporating Uncertainty

Junjie Li, Kong Aik Lee, *Senior Member, IEEE*

Abstract—An utterance-level speaker embedding is typically obtained by aggregating a sequence of frame-level representations. However, in real-world scenarios, individual frames encode not only speaker-relevant information but also various nuisance factors. As a result, different frames contribute unequally to the final utterance-level speaker representation for Automatic Speaker Verification systems. To address this issue, we propose to estimate the inherent uncertainty of each frame and assign adaptive weights accordingly, where frames with higher uncertainty receive lower attention. Based on this idea, we present \mathcal{U}^3 -xi, a comprehensive framework designed to produce more reliable and interpretable uncertainty estimates for speaker embeddings. Specifically, we introduce several strategies for uncertainty supervision. First, we propose *speaker-level uncertainty supervision* via a *Stochastic Variance Loss*, where the distance between an utterance embedding and its corresponding speaker centroid serves as a pseudo ground truth for uncertainty learning. Second, we incorporate *global-level uncertainty supervision* by injecting the predicted uncertainty into the *softmax* scale during training. This adaptive scaling mechanism adjusts the sharpness of the decision boundary according to sample difficulty, providing global guidance. Third, we redesign the uncertainty estimation module by integrating a Transformer encoder with *multi-view self-attention*, enabling the model to capture rich local and long-range temporal dependencies. Comprehensive experiments demonstrate that \mathcal{U}^3 -xi is model-agnostic and can be seamlessly applied to various speaker encoders. In particular, when applied to ECAPA-TDNN, it achieves 21.1% and 15.57% relative improvements on the VoxCeleb1 test sets in terms of EER and minDCF, respectively.

Index Terms—Speaker Recognition, Uncertainty Supervision, Scale

I. INTRODUCTION

AUTOMATIC speaker verification (ASV) aims to determine a speaker’s identity solely from their voice using machine learning algorithms and is one of the most convenient and natural forms of biometric authentication [1]. ASV systems are designed to extract speaker-discriminative information while suppressing nuisance factors such as linguistic content, emotional variation, and background noise [2]. Beyond biometric authentication, ASV supports a wide range of applications, including personalized user services [3] as well as security and surveillance scenarios [4]. Moreover, speaker modeling techniques developed for ASV are fundamental to various downstream tasks, such as target speaker extraction [5], speech synthesis [6], and voice conversion [7], where high-quality speaker embeddings are indispensable.

Junjie Li and Kong Aik Lee are with the Department of Electrical and Electronic Engineering, Faculty of Engineering, The Hong Kong Polytechnic University, Hong Kong SAR, China (email: junjie98.li@connect.polyu.hk, kong-aik.lee@polyu.edu.hk).

A typical speaker recognition system consists of three modules: a front-end speaker encoder, a pooling layer, and a classifier. The speaker encoder transforms the input speech waveform into a sequence of frame-level embeddings. However, speech is inherently complex and contains not only speaker traits but also numerous non-speaker variations [2]. To summarize the temporal sequence into a fixed-dimensional representation, the pooling layer aggregates frame embeddings with different weights assigned to different frames. Although many pooling strategies have been proposed [8]–[17], most approaches still overlook data uncertainty, which has been shown to be beneficial across multiple domains [18]–[30].

Recently, Lee et al. [24] introduced uncertainty estimation into deep neural networks for ASV through the xi-vector model. This approach applies Gaussian posterior inference to aggregate temporal frame-level features into an utterance-level speaker embedding while simultaneously estimating uncertainty. Despite its success, the xi-vector framework still exhibits several limitations that restrict the reliability of its uncertainty estimation. First, the uncertainty estimation module consists of only two shallow linear layers, which may lack sufficient modeling capacity to capture complex non-linear relationships across temporal frames. Second, the xi-vector is trained solely with a cross-entropy (CE) loss, for which the uncertainty is learned implicitly through classification supervision alone, without any explicit guidance or direct supervision on the uncertainty estimate itself. This leads to sub-optimal uncertainty modeling and reduces robustness in real-world scenarios.

To address the above limitations, we propose a series of improvements aimed at producing more reliable and interpretable uncertainty estimation:

- **Speaker-level Uncertainty Supervision.** We use stochastic estimate of embedding deviation as a pseudo-ground truth target to explicitly supervise the predicted uncertainty. This forms our *Stochastic Variance Loss* (SVL). Furthermore, the predicted uncertainty is incorporated into the cosine scoring function, leading to an *uncertainty-aware cosine scoring* scheme. Together, these components yield nearly a 5% relative improvement in performance compared to the conventional xi-vector.
- **Global-level Uncertainty Supervision.** Speaker-level supervision provides guidance only among utterances belonging to the same speaker, but it fails to compare uncertainty across different speakers. To address this limitation, we introduce global-level uncertainty supervision by introducing uncertainty into the scale parameter of the *softmax* function. The scale dynamically adapts

to sample difficulty, making the *softmax* distribution sharper for easy samples and smoother for hard ones. Through this mechanism, uncertainty is explicitly learned at the global distribution level, resulting in a 3.45% relative improvement in performance compared to the conventional xi-vector.

- **Uncertainty Estimation Module.** To enhance the modeling capacity of uncertainty estimation, we incorporate a Transformer encoder [31] into the uncertainty estimation module. The self-attention mechanism significantly improves the network’s ability to model complex non-linear relationships and capture long-range temporal dependencies—capabilities that shallow linear layers inherently lack. Furthermore, to better encode short to long range temporal structures, we extend standard multi-head self-attention (MHA) to a *multi-view self-attention* (MVA) [32] design. This extension enables richer and more robust variance estimation across both short- and long-range temporal dependencies, resulting in a 5.48% relative improvement in performance compared to xi-vector.

Each of the proposed enhancements contributes to performance improvement. When combined, they yield a substantial cumulative gain, achieving 21.1% and 15.57% relative improvements in terms of EER and minDCF, respectively, compared with the ECAPA-TDNN model.

II. RELATED WORK

A. Uncertainty Estimation in Deep Learning

In general, uncertainty can be categorized into two types: epistemic and aleatoric [33]–[35]. *Epistemic uncertainty* arises from the model or its parameters, representing the model’s lack of knowledge. For instance, when the input lies outside the training distribution, the model should exhibit high epistemic uncertainty. In contrast, *aleatoric uncertainty* originates from the data itself, reflecting inherent noise or ambiguity. A higher aleatoric uncertainty indicates that the data contain greater noise or variability. Similar to [24], this paper focuses exclusively on the uncertainty intrinsic to the data. Therefore, unless otherwise specified, the term uncertainty refers to *aleatoric uncertainty*.

In real-world scenarios, data are rarely perfectly clean. They may contain irrelevant information, background noise, or even incorrect labels, all of which contribute to varying degrees of data uncertainty. Such uncertainty arises from multiple sources and can manifest differently across modalities, such as speech and visual data. Effectively modeling this uncertainty is essential for improving the robustness and interpretability of deep neural networks (DNNs) [18]–[23]. These studies introduced Gaussian representations in the latent space encoded by DNNs, where the variance serves as an estimate of the uncertainty.

In speaker recognition task, the xi-vector model [24] was proposed to estimate the uncertainty of each speech frame using deep neural networks (DNNs), inspired by the successful treatment of uncertainty in the *universal background model* (UBM) [25] and the i-vector framework [26]. Similar concepts have been widely adopted and shown effective in related areas

such as speech disentanglement [27], voice anonymization [28]–[30], and speaker verification [36]–[39].

B. Large Margin Softmax Loss Function

Large margin softmax loss functions have been extensively studied and demonstrated to be highly effective in both face recognition [40]–[46] and speaker verification tasks [47]–[50]. By introducing an angular or additive margin to the target class, these losses enforce stricter separation between classes and encourage intra-class compactness and inter-class discrimination. Early works such as SphereFace [41] introduced multiplicative angular margins, while subsequent methods, including CosFace (additive cosine margin) [42] and ArcFace (additive angular margin) [43], further improved the geometric interpretability and optimization stability of margin constraints. In the speaker verification domain, large margin softmax variants (e.g., AAM-Softmax [43], AM-Softmax [42]) have become standard training objectives due to their ability to produce highly discriminative speaker embeddings.

In addition to margin manipulation, several studies [51], [52], [52]–[56] have explored the role of the scale parameter, which controls the sharpness of the class posterior distribution produced by the output of the softmax layer. A larger scale magnifies the logit differences, yielding a sharper posterior distribution and stronger class separation. However, it may also cause over-confidence when the embeddings are unreliable. Conversely, a smaller scale smooths the posterior distribution and stabilizes gradients, especially under challenging acoustic conditions, though at the cost of reduced discriminability. This is because a smaller scale dampens the logit values sent to the softmax layer, making extreme probabilities (near 0 or 1) less common. With fewer extreme probabilities, the loss function’s gradients change more gradually during training, avoiding sharp fluctuations or vanishing gradients that could disrupt learning. Different works leverage this trade-off in distinct ways. It has been observed that using a smaller scale can enhance adversarial robustness [53], whereas AdaCos [54] adopts a dynamic scale that gradually decreases throughout training. In contrast, other works increase the scale dynamically, arguing that a larger scale facilitates learning of hard samples [51], [55]. Beyond fixed or manually designed schedules, some methods propose predicting a sample-wise scale using DNNs [52], [56]. In these approaches, the learned scale can be interpreted as a *quality* or *uncertainty* indicator, with higher predicted scales corresponding to cleaner or more easily classifiable samples, and lower scales reflecting higher uncertainty or degraded quality.

C. Temporal Pooling Layers

Temporal pooling plays a critical role in speaker embedding extraction. It aggregates sequences of frame-level features into utterance-level representations, from which the final speaker embeddings are derived [2], [57]. Existing temporal pooling approaches range from relatively simple statistical methods to more sophisticated techniques incorporating attention mechanisms. Statistical pooling methods summarize the frame sequence using global statistics. Temporal Average Pooling (TAP) [8] computes the mean of frame-level deep features to

represent the utterance-level embedding. Temporal Statistics Pooling (TSTP) [9] extends TAP by concatenating the mean and standard deviation vectors, thereby incorporating variance information. Temporal Standard Deviation Pooling (TSDP) [10] demonstrates that even using only the standard deviation vector can remain effective.

However, traditional statistical pooling assumes that all frames contribute equally to the utterance-level representation, which is often not the case in practice. Frame-level features may vary in their speaker-discriminative importance, motivating the use of attention mechanisms to weight frames differently. Attentive Statistics Pooling (ASP) [11] addresses this issue by computing both weighted mean and weighted standard deviation vectors. Subsequent studies [12]–[15] demonstrate that multi-head attention further improves pooling performance. ECAPA-TDNN [16] advances this idea by extending attention to the channel dimension, allowing the model to emphasize speaker characteristics that do not activate at the same temporal positions.

In the xi-vector model [24], attention-based weighting is replaced by a sequence of frame-level uncertainty estimates, where higher uncertainty corresponds to a lower contribution to the utterance-level representation. As adopted in this paper, this uncertainty-aware pooling strategy provides a principled and interpretable mechanism for down-weighting unreliable frames while preserving speaker-discriminative information.

III. BACKGROUND

A. Uncertainty-aware Speaker Model: xi-vector

In speaker recognition tasks, generating compact and discriminative embeddings is essential for representing speaker characteristics across speech utterances of varying length. The xi-vector framework [24], [37], [38] introduces a novel temporal pooling mechanism based on Gaussian posterior inference, which aggregates frame-level features into a fixed-dimensional utterance embedding while weighting each frame according to its estimated uncertainty.

As illustrated in Fig. 1, the Gaussian posterior inference serves as a generalizable pooling module that can be integrated into any speaker encoder architecture. Given an input speech sequence $X = \{x_1, x_2, \dots, x_T\}$ of T frames, a speaker encoder first transforms it into a sequence of frame-level representations $\{\mathbf{z}_1, \mathbf{z}_2, \dots, \mathbf{z}_T\}$. In addition, the model estimates the uncertainty associated with each frame, expressed as the log-precision $\log \mathbf{L}_t$, where higher precision denotes lower uncertainty. To maintain computational efficiency, the precision matrix \mathbf{L}_t is assumed to be diagonal in practice. From the perspective of a linear Gaussian model, the observed representation \mathbf{z}_t can be decomposed into two components:

$$\mathbf{z}_t = \mathbf{h} + \boldsymbol{\epsilon}_t, \quad (1)$$

where $\mathbf{h} \sim \mathcal{N}(\boldsymbol{\mu}_p, \mathbf{L}_p^{-1})$ ¹ denotes the latent speaker variable shared across the entire sequence, and $\boldsymbol{\epsilon}_t \sim \mathcal{N}(0, \mathbf{L}_t^{-1})$ represents the frame-specific random variable capturing uncertainty

¹The quantities $\boldsymbol{\mu}_p$ and \mathbf{L}_p^{-1} denote the prior mean and prior covariance matrix, respectively. They are initialized as 0 and 1. For notational consistency with the frame-level representations \mathbf{z}_t , we also denote the prior mean $\boldsymbol{\mu}_p$ as \mathbf{z}_p in the subsequent sections. Both symbols refer to the same quantity.

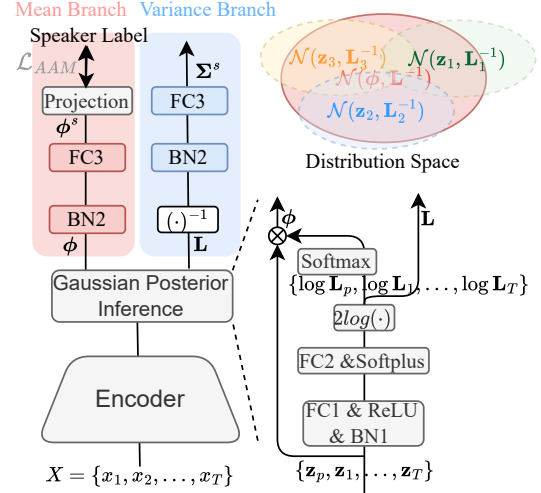


Fig. 1. Architecture of the xi-vector model with integrated uncertainty estimation. The mean and variance branches share the same parameters but apply different operations, reflecting the distinct mathematical formulations of mean and variance from a statistical perspective.

at time t , respectively. Given current observation sequence, the posterior distribution of \mathbf{h} is estimated as follow:

$$p(\mathbf{h}|\mathbf{z}_1, \dots, \mathbf{z}_T, \mathbf{L}_1^{-1}, \dots, \mathbf{L}_T^{-1}) = \mathcal{N}(\mathbf{h}|\boldsymbol{\phi}, \mathbf{L}^{-1}). \quad (2)$$

By considering its prior mean and covariance, the posterior mean and covariance could be computed as:

$$\boldsymbol{\phi} = \frac{\sum_{t=1}^T \mathbf{L}_t \mathbf{z}_t + \mathbf{L}_p \mathbf{z}_p}{\mathbf{L}} \text{ and} \quad (3)$$

$$\mathbf{L}^{-1} = \left(\sum_{t=1}^T \mathbf{L}_t + \mathbf{L}_p \right)^{-1}. \quad (4)$$

Then, the posterior mean $\boldsymbol{\phi}$ and covariance \mathbf{L}^{-1} are propagated through a batch normalization layer followed by a fully connected layer to obtain the final speaker embedding. Following the property of Gaussian distribution $\mathcal{N}(\mathbf{h}|\boldsymbol{\phi}, \mathbf{L}^{-1})$, where the transform on \mathbf{h} is applied conserving its mean and covariance matrix. This is implemented as shown in Fig. 1. The parameters of these layers are shared between the mean branch and the variance branch, but different statistical operations are applied in each branch [30], [37].

For the mean branch, the transformation can be expressed as² :

$$\boldsymbol{\phi}^s = \left(\frac{\boldsymbol{\phi} - \boldsymbol{\mu}_{bn}}{\sqrt{\sigma_{bn} + \epsilon \mathbf{I}}} \otimes \boldsymbol{\gamma}_{bn} + \boldsymbol{\beta}_{bn} \right) \mathbf{A}_{fc}^\top + \mathbf{b}_{fc}, \quad (5)$$

where $\boldsymbol{\mu}_{bn}$ and σ_{bn} denote the batch-wise mean and variance in batch normalization, respectively. The parameter ϵ is a small constant for numerical stability, and $\boldsymbol{\gamma}_{bn}$ and $\boldsymbol{\beta}_{bn}$ are learnable affine parameters. The symbol \otimes denotes element-wise multiplication. Finally, \mathbf{A}_{fc} and \mathbf{b}_{fc} are the learnable parameters of the fully connected layer.

For the variance branch, the same set of parameters as in the mean branch is used, but with a different computational formulation in order to model the covariance:

$$\Sigma^s = \mathbf{A}_{fc} \frac{\mathbf{L}^{-1} \otimes \boldsymbol{\gamma}_{bn}^2}{\sigma_{bn} + \epsilon \mathbf{I}} \mathbf{A}_{fc}^\top. \quad (6)$$

²These equations are written in PyTorch style for clarity, similar to <https://docs.pytorch.org/docs/stable/generated/torch.nn.BatchNorm1d.html>.

B. Softmax in Speaker Classification

As shown in Fig. 1, the projection layer maps the utterance-level representation ϕ^s into a C -dimensional vector, where C is the number of speakers in the training set. This vector is then optimized using a classification objective, with the softmax function playing a central role.

1) *Softmax*: To begin with, we briefly recall the standard softmax loss, which is widely used in speaker recognition. It is defined as:

$$\mathcal{L}_S = -\frac{1}{N} \sum_{i=1}^N \log \frac{e^{\mathbf{W}_{y_i}^\top \phi_i^s + \mathbf{b}_{y_i}}}{\sum_{j=1}^C e^{\mathbf{W}_j^\top \phi_i^s + \mathbf{b}_j}}, \quad (7)$$

where N is the number of training samples, C denotes the total number of training classes, ϕ_i^s represents the embedding of the i -th utterance, and \mathbf{W}_j together with \mathbf{b}_j corresponds to the classifier weight and bias for the j -th class, respectively. The term $\mathbf{W}_{y_i}^\top \phi_i^s + \mathbf{b}_{y_i}$ is commonly referred to as the target logit of the i -th sample, where y_i indicates its ground-truth class.

2) *Additive Angular Margin Softmax*: While the conventional Softmax loss serves as a basic classification objective, it does not explicitly encourage the learned embeddings to be both intra-class compact (features from the same class clustering tightly together) and inter-class separable (features from different classes being well apart). To overcome this limitation, the Additive Angular Margin Softmax (AAM-Softmax) loss [43] was proposed. This formulation strengthens discriminative power by introducing an angular margin penalty.

Specifically, AAM-Softmax first removes the bias term ($\mathbf{b} = 0$) and reformulates the logit as $\mathbf{W}^\top \phi^s = \|\mathbf{W}\| \|\phi^s\| \cos \theta$, where θ is the angle between the class weight \mathbf{W} and the feature embedding ϕ^s . Furthermore, to ensure that the prediction depends solely on the angular similarity rather than the vector magnitude, both \mathbf{W} and ϕ^s are normalized:

$$\hat{\mathbf{W}} = \frac{\mathbf{W}}{\|\mathbf{W}\|}, \quad \hat{\phi}^s = \frac{\phi^s}{\|\phi^s\|}. \quad (8)$$

With these normalizations, the classification is determined by the cosine similarity. To further enhance discriminability, an additive angular margin m is imposed on the target logit, leading to the following loss function:

$$\mathcal{L}_{\text{AAM}} = -\frac{1}{N} \sum_{i=1}^N \log \frac{e^{s \cos(\theta_{y_i} + m)}}{e^{s \cos(\theta_{y_i} + m)} + \sum_{j=1, j \neq y_i}^C e^{s \cos \theta_j}}, \quad (9)$$

where s is a fixed scaling factor that stabilizes optimization, and m is the angular margin encouraging tighter intra-class clusters and larger inter-class separation.

IV. SPEAKER-LEVEL UNCERTAINTY SUPERVISION

A. Stochastic Variance Loss

Our previous work xi-vector [24] relies solely on a classification loss to *implicitly* supervise frame-level uncertainty, without any form of explicit guidance. Such implicit learning often results in suboptimal or unstable uncertainty estimation.

To overcome this limitation, we introduce an *explicit* supervision mechanism for utterance-level uncertainty modeling, termed *Stochastic Variance Loss* (SVL). Our previous work [36] firstly proposed SVL in the context of speaker recognition and demonstrated its effectiveness. In this paper, we further generalize this idea by exploring other alternative formulations to realize the core concept of SVL.

The proposed loss \mathcal{L}_{SVL} aims to establish a pseudo ground truth for utterance-level uncertainty estimation. Specifically, we treat the distance between the centroid of embeddings from the same speaker and the current utterance's embedding ϕ^s as a pseudo label. Since only the embedding distance of a single utterance-centroid pair is used to approximate the uncertainty (i.e., variance), we refer to this approach as *stochastic variance learning*.

Suppose we use $\phi_{y_i}^c$ to represent the centroid of speaker y_i of utterance i :

$$\phi_{y_i}^c = \frac{\sum_{i=1}^I \phi_i^s}{I}, \quad (10)$$

where all I utterances belong to the same speaker y_i . The the \mathcal{L}_{SVL} is given by:

$$\mathcal{L}_{\text{SVL}} = \frac{1}{B} \sum_{b=1}^B \|\alpha(\Sigma_b^s)^{\frac{1}{2}} - \|\phi_b^s - \phi_{y_b}^c\|^2\|^2, \quad (11)$$

where B denotes the number of batch size in training. Σ_b^s and $\phi_{y_b}^c$ denote the covariance matrix for utterance b and the centroid of speaker y_b , respectively. $\|\cdot\|$ denotes the Euclidean norm. In addition, α is a learnable parameter initialized from 1, reference to as the uncertainty scaling factor, aiming to address potential scale mismatch between predicted uncertainty and pseudo ground truth.

There are two strategies for computing the centroid:

- **Pre:** The centroid is computed using embeddings ϕ^s extracted from a pre-trained model with the same architecture. But this pre-trained model is trained solely with the cross-entropy loss \mathcal{L}_{AAM} , without the proposed \mathcal{L}_{SVL} . As a result, the speaker centroids remain fixed throughout training and are subsequently used to provide supervision, as defined in Eq. (11).
- **Epoch:** Instead of relying on a pre-trained model, the speaker embedding ϕ^s is extracted using the checkpoint from the last epoch. Then then centroid is computed and updated after each training epoch. This allows the centroid representations to evolve along with model optimization, leading to progressively more accurate speaker representations.

The final training loss is given by:

$$\mathcal{L}_{\text{Final}} = \mathcal{L}_{\text{AAM}} + \kappa \mathcal{L}_{\text{SVL}}, \quad (12)$$

where κ is used to control loss weight and is dynamically adjusted based on the current epoch ep to ensure that \mathcal{L}_{SVL} gradually contributes as training progresses:

$$\kappa = \begin{cases} 0, & \text{if epoch} \leq \text{eps}_{\text{SVL}}, \\ \lambda \frac{ep - \text{eps}_{\text{SVL}}}{ep_{\text{Max}} - \text{eps}_{\text{SVL}}}, & \text{otherwise,} \end{cases} \quad (13)$$

where λ is a pre-defined fixed constant, eps_{SVL} indicates epoch when \mathcal{L}_{SVL} starts to be applied. ep_{Max} indicates the maximum

number of training epochs. In this paper, we set $eps_{SVL} = 40$ and $ep_{Max} = 150$. Cause we use WeSpeaker [58], [59] as training tool, its margin changes before 40 epoch, which causes unstable training and produces NaN if we incorporate \mathcal{L}_{SVL} at this stage.

B. Uncertainty-aware Scoring

Since the uncertainty varies across utterances, it is intuitive to incorporate uncertainty into the scoring backend. In this work, we adopt cosine similarity as the scoring metric, which is computed as follows:

$$s_u = \frac{\langle \phi_2^s, \phi_1^s \rangle}{\sqrt{\phi_2^s \top (\mathbf{I} + \rho \Sigma_2^s)^{-1} \phi_2^s} \sqrt{\phi_1^s \top (\mathbf{I} + \rho \Sigma_1^s)^{-1} \phi_1^s}}, \quad (14)$$

where ρ denotes a scaling factor in cosine scoring, and \mathbf{I} is the identity matrix. The subscripts 1 and 2 indicate the corresponding speaker identities for the enrollment and test embeddings, respectively. When the covariance matrix Σ^s or ρ is zero, the uncertainty-aware cosine scoring s_u reduces to the normal cosine similarity. Wang et al. [38] have proposed to use the fixed constant $1/d$ as ρ , where d denotes the dimension of speaker embedding. However, a fixed value may not be optimal, as demonstrated in our previous work, xi+ [36]. To address this limitation, we introduce a learnable uncertainty scaling factor α , which replaces ρ in uncertainty-aware scoring. This parameter can be adapted to different training datasets, allowing the model to optimally calibrate the influence of uncertainty in the scoring process.

V. GLOBAL-LEVEL UNCERTAINTY SUPERVISION

Speaker-level uncertainty supervision can only compare uncertainty among utterance embeddings of the same speaker. For embeddings belonging to different speakers, the SVL does not provide a direct or meaningful basis for comparison. In this section, we introduce a global-level uncertainty supervision mechanism, which evaluates and constrains uncertainty across embeddings from all utterances in the training set, rather than being limited to within-speaker comparisons.

A. Uncertainty-aware Softmax

Conventional Softmax-based objectives (e.g., Eq. 7 and Eq. 9) operate solely on the deterministic embedding ϕ^s , which represents only a point estimate of the speaker identity. Such formulations overlook the covariance information Σ^s , thereby discarding valuable information about embedding reliability.

To address this limitation, we reformulate the normalization equation 8 by incorporating the uncertainty term, the uncertainty-aware normalized embedding is given by:

$$\tilde{\phi}^s = \frac{\sqrt{\phi^s \top (\Lambda + \Sigma^s)^{-1} \phi^s}}{\|\phi^s\|}, \quad (15)$$

which normalizes the embedding under the Mahalanobis metric induced by the uncertainty covariance $\Lambda + \Sigma^s$ where Λ is a bias term that enhances numerical stability to avoid small denominators. This formulation ensures that $\tilde{\phi}^s$ is a unit vector in the uncertainty-aware space, reflecting both its magnitude and its uncertainty structure. However, in practice, explicitly

computing the inverse $(\Lambda + \Sigma^s)^{-1}$ often leads to unstable gradients or NaN values during training. To mitigate this issue, we adopt a numerically stable alternative:

$$\tilde{\phi}^s = \frac{\|\phi^s\|}{\sqrt{\phi^s \top (\Lambda + \Sigma^s) \phi^s}}. \quad (16)$$

These two expressions are closely related. We visualize their values in Fig. 2, where both the bias term Λ and the embeddings ϕ are generated randomly. The figure demonstrates that the trends of the two equations are similar, with the primary difference being their absolute values. Moreover, as the mean variance increases, the discrepancy between the two expressions also tends to grow.

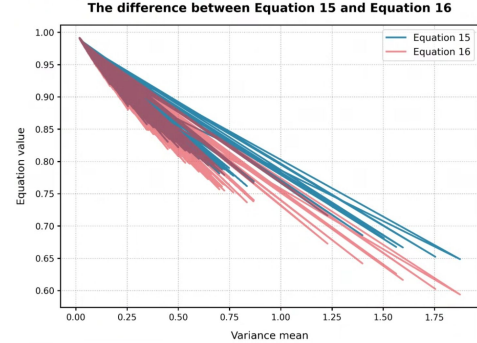


Fig. 2. The value difference between Equation 15 and Equation 16.

Furthermore, this second, stable expression can be decomposed into two distinct components:

$$\tilde{\phi}^s = \frac{\phi^s}{\|\phi^s\|} \cdot \frac{\|\phi^s\|}{\sqrt{\phi^s \top (\Lambda + \Sigma^s) \phi^s}}, \quad (17)$$

$$= \hat{\phi}^s \cdot s_u, \quad (18)$$

where $\hat{\phi}^s$ is a unit-norm embedding and $s_u > 0$ is referred to as the uncertainty-aware scale. Crucially, this scale **increases** as the uncertainty **decreases**, effectively modulating the embedding's magnitude based on the uncertainty of its estimate. We then incorporate the uncertainty-aware embedding $\tilde{\phi}^s$ into the AAM-Softmax formulation to obtain the uncertainty-aware AAM-Softmax (AAM_u):

$$\mathcal{L}_{\text{AAM}_u} = -\frac{1}{N} \sum_{i=1}^N \log \frac{e^{s \cdot s_u \cos(\theta_{y_i} + m)}}{e^{s \cdot s_u \cos(\theta_{y_i} + m)} + \sum_{j=1, j \neq y_i}^C e^{s \cdot s_u \cos(\theta_j)}}. \quad (19)$$

B. Gradient-Driven Adaptation of Scale and Covariance

From a training perspective, the uncertainty-aware scale s_u allows the model to adjust its confidence dynamically based on the reliability of each embedding. For an unreliable sample, typically corresponding to a large loss, the optimizer naturally encourages the model to reduce scale during back-propagation [52], [56]. A smaller scale softens the softmax distribution, reducing the penalty from incorrect or ambiguous logits and preventing the model from making overly confident but potentially wrong predictions. In our design, decreasing s_u directly corresponds to increasing the predicted variance

(uncertainty), which aligns with intuitive expectations: harder samples should be associated with higher uncertainty.

Conversely, for reliable samples with small loss, the gradient pushes s_u upward. This sharpens the softmax distribution, enhancing the separation between target and non-target classes, and leads to smaller predicted uncertainty. In this way, the proposed scale-variance mechanism provides a training-driven confidence adjustment: for hard samples, which correspond to large losses, the back-propagation gradient drives the model to decrease the uncertainty-aware scale s_u . As a result, the predicted variance Σ^s increases, reflecting the higher uncertainty of these embeddings. Conversely, for easy samples with small loss, the gradient encourages s_u to increase, leading to smaller Σ^s , as shown in Fig. 3.

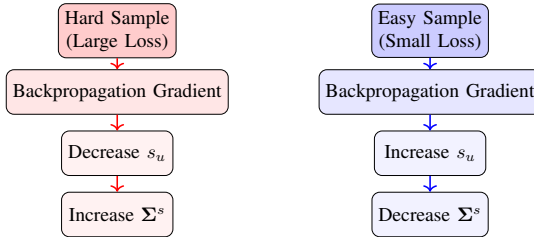


Fig. 3. Illustration of how the uncertainty adjusts based on sample difficulty.

VI. UNCERTAINTY ESTIMATION MODULE

The previous two sections focus on modifying the training strategies without altering the model architecture. In this section, we aim to redesign the uncertainty estimation module. Our previous work xi-vector [24], the uncertainty estimation relies on two simple learnable layers with basic activation functions to predict frame-level uncertainty, as illustrated in Fig. 1. However, this design is relatively shallow and lacks the ability to capture temporal dependencies across speech frames. Our previous work [36] addressed this limitation by incorporating a Transformer encoder to explicitly model temporal relations, thereby enhancing the model’s capacity to capture complex non-linear patterns. Although Transformer-based architectures have been explored for speaker recognition, they often struggle to adequately capture short-range local context [32], [60]–[62]. Among the proposed variants, multi-view self-attention (MVA) [32] is particularly noteworthy: each attention head is assigned a distinct temporal window, enabling it to focus on different receptive-field ranges. This design simultaneously enhances the modeling of global dependencies and strengthens the ability to capture local contextual patterns. Such a property aligns well with our goal, as it allows the uncertainty estimation module to effectively capture both long-range dependencies and fine-grained local patterns, which are essential for robust and reliable uncertainty estimation, as shown in Fig. 4. For each attention head, the receptive-field size is defined as:

$$w_h = 2^{(h+1)} + 1, \quad (20)$$

where $h \in \{0, \dots, H-1\}$ denotes the head index among a total of H heads, and w_h represents the full temporal window size for the h -th head.

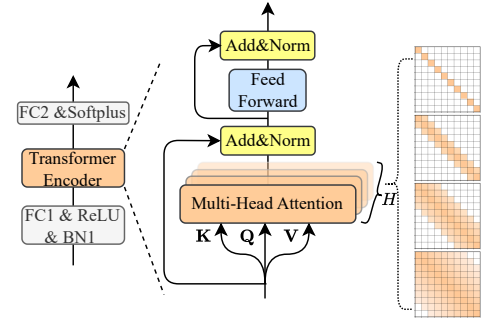


Fig. 4. The proposed uncertainty estimation module. Temporal relationships are modeled by a Transformer encoder, and each attention head is assigned with a distinct temporal window, offering multi-view perspectives for estimating frame-level uncertainty.

VII. EXPERIMENTAL SETUP

A. Dataset

All models are trained on VoxCeleb2 [63] and evaluated on the in-domain VoxCeleb1 test set [64], as well as on cross-domain test sets including Speakers in the Wild (SITW) [65] and CNCeleb [66]³. Data augmentation is applied during training using additive noise from the MUSAN corpus [67] and simulated reverberation via room impulse responses from the RIR database [68].

B. Training Strategy

We adopt the training pipeline from the VoxCeleb v2 recipe provided by the WeSpeaker toolkit⁴ [58], following all default hyperparameter settings. The training spans 150 epochs, using 2-second audio segments. The default scale s in AAM-softmax and is 32. The angular margin is initially set to zero and then progressively increased from 0 to 0.2 between epochs 20 and 40, after which it remains fixed. Finally, we average the parameters from the last 10 checkpoints to obtain a final model checkpoint. Unless otherwise specified, ECAPA-TDNN [16] is adopted as the default speaker encoder.

VIII. RESULTS AND DISCUSSIONS

A. Visualization of Uncertainty Estimation

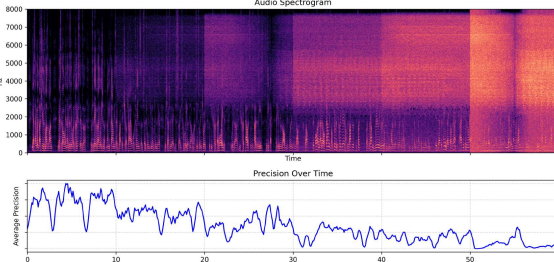
Unlike previous temporal pooling layers that rely on statistical operators or attention mechanisms, we explicitly estimate the covariance of each frame based on Gaussian posterior inference and use it as an importance weight. A larger covariance indicates that the corresponding frame is less reliable and contributes less to the final utterance-level speaker embedding.

To verify that the estimated covariance indeed aligns with our objective, we visualize the temporal variation of the precision matrix (i.e., the inverse of the covariance matrix). Specifically, we average the precision matrix along the channel dimension and plot its values over time, as shown in Fig. 5. The input utterance is 60 seconds long, and we apply two types of distortions: adding noise and masking regions of the spectrogram. From the two visualizations, we observe that the

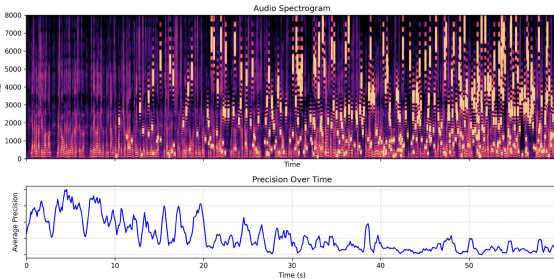
³For SITW, the core–core condition is used. For CNCeleb, the evaluation list from CNC-Eval-Avg in WeSpeaker [58] is adopted.

⁴<https://github.com/wenet-e2e/wespeaker/blob/master/examples/voxceleb/v2/run.sh>

⁵Results come from <https://github.com/wenet-e2e/wespeaker/blob/master/examples/voxceleb/v2/README.md>



(a) Frame-wise precision under varying SNR conditions. The SNR levels for the intervals 0–10 s, 10–20 s, 20–30 s, 30–40 s, 40–50 s, and 50–60 s are clean, 20 dB, 10 dB, 0 dB, -10 dB, and -20 dB, respectively.



(b) Frame-wise precision under different spectrogram patch masking levels. From left to right, increasingly larger portions of the spectrogram are masked.

Fig. 5. Comparison of frame-wise precision under (a) noise corruption and (b) spectrogram masking conditions.

precision values decrease as the speech becomes more severely corrupted. Moreover, even regions containing weak or sparse speech exhibit lower precision, indicating reduced reliability. These observations confirm that the estimated frame-level uncertainty effectively reflects the quality and trustworthiness of the speech signal.

B. The Effectiveness of Speaker-level Uncertainty Supervision

We have shown that the frame-level uncertainty estimation within an utterance is accurate. However, because the model applies a *softmax* function to normalize uncertainty scores

within each utterance, the utterance-level uncertainty Σ^s is not explicitly supervised or constrained, and may therefore be unreliable. Therefor, we propose speaker-level uncertainty supervision mechanism and verify the effectiveness of it in this section.

As shown in Table I, we compare the performance of our two *Stochastic Variance Loss* variants, $\mathcal{L}_{\text{SVL-Pre}}$ and $\mathcal{L}_{\text{SVL-Epoch}}$. The results indicate that using \mathcal{L}_{SVL} alone does not yield noticeable improvements. However, combining it with the *uncertainty-aware* cosine scoring function leads to better performance. We further evaluate two strategies for the scaling factor ρ : (1) the static factor $1/d$ proposed by Wang [38], and (2) a learnable factor α trained jointly with the model. Results demonstrate that the learnable scaling factor significantly outperforms the static counterpart. When combining \mathcal{L}_{SVL} with the learnable scaling factor α , consistent and significant improvements are observed across different loss weights λ . We further evaluate the models on a cross-domain test set, as shown in Fig. 6. Exps. 3–5 consistently outperform the two baseline methods across all metrics, whereas Exps. 6–8 exhibit unstable behavior and, in some cases, even underperform compared to the baselines. These results indicate that $\mathcal{L}_{\text{SVL-Pre}}$ is more effective, providing stronger robustness and better generalization to unseen domains. Additionally, Exp. 4 with $\lambda = 0.05$ achieves the best overall performance.

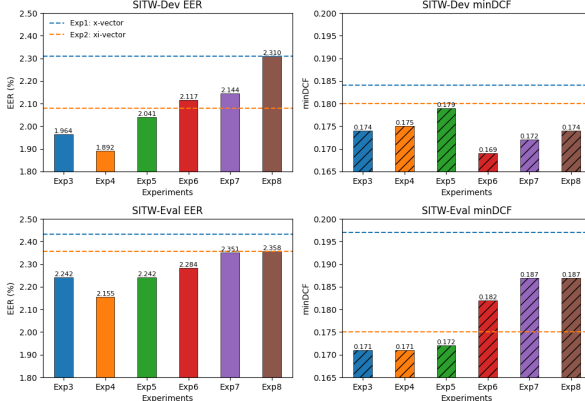
C. The Effectiveness of Global-level Uncertainty Supervision

Speaker-level supervision constrains uncertainty only within utterances from the same speaker and cannot compare uncertainty across different speakers. In practice, however, each training sample produces a different loss value, reflecting its varying difficulty. These loss differences are back-propagated to the uncertainty-aware scale s_u in $\mathcal{L}_{\text{AAM}_u}$, causing the scale to update dynamically. Since the scale embeds the uncertainty term, this dynamic adjustment naturally induces global-level uncertainty supervision across all samples, enabling the model to learn consistent uncertainty behavior beyond individual

TABLE I

OVERALL RESULTS ON VOXCELEB1 IN TERMS OF THE EER (%) AND minDCF WHERE LOWER VALUES INDICATE BETTER PERFORMANCE. ALL EXPERIMENTS IN THIS TABLE EMPLOY ECAPA-TDNN [16] AS THE SPEAKER ENCODER. Δ DENOTES RELATIVE IMPROVEMENT COMPARED TO THE BENCHMARK.

#Exp.	Model	#Param.	\mathcal{L}_{SVL}		Uncertainty Scoring ρ	Vox1-O		Vox1-E		Vox1-H		Avg. Δ
			Method	λ		EER	minDCF	EER	minDCF	EER	minDCF	
1 ⁵	x-vector [16]	6.19 M	$\mathcal{L}_{\text{SVL-Pre}}$	0	0	1.069	0.122	1.209	0.136	2.310	0.226	Benchmark
2	xi-vector [24]	5.90 M			0.995	0.103	1.130	0.126	2.169	0.209		
					0.989	0.100	1.123	0.125	2.158	0.208	1.00%	
3	xi-vector+ \mathcal{L}_{SVL}	5.90 M	$\mathcal{L}_{\text{SVL-Pre}}$	0.01	0	1.048	0.126	1.142	0.128	2.202	0.205	-4.95%
					1/d [38]	1.053	0.124	1.137	0.128	2.195	0.204	-4.57%
					0.994	0.103	1.080	0.117	2.088	0.201	3.21%	
4			$\mathcal{L}_{\text{SVL-Epoch}}$	0.05	0	1.021	0.108	1.139	0.128	2.176	0.205	-1.71%
					1/d	1.005	0.107	1.135	0.127	2.164	0.204	-0.58
					0.936	0.100	1.076	0.116	2.068	0.202	4.92%	
5			$\mathcal{L}_{\text{SVL-Pre}}$	0.1	0	1.042	0.115	1.150	0.127	2.204	0.209	-3.43%
					1/d	1.042	0.114	1.148	0.127	2.200	0.205	-2.88%
					0.994	0.101	1.103	0.119	2.113	0.198	2.98%	
6	xi-vector+ \mathcal{L}_{SVL}	5.90 M	$\mathcal{L}_{\text{SVL-Epoch}}$	0.01	0	1.064	0.114	1.157	0.127	2.163	0.211	-3.57%
					1/d	1.053	0.111	1.150	0.126	2.154	0.210	-2.53%
					0.931	0.102	1.079	0.115	2.046	0.201	5.02%	
7			$\mathcal{L}_{\text{SVL-Pre}}$	0.05	0	1.064	0.117	1.160	0.125	2.155	0.210	-3.70%
					1/d	1.063	0.115	1.155	0.125	2.148	0.208	-2.74%
					0.952	0.099	1.095	0.117	2.053	0.198	4.84%	
8			$\mathcal{L}_{\text{SVL-Epoch}}$	0.1	0	1.032	0.117	1.161	0.126	2.161	0.212	-3.52%
					1/d	1.031	0.115	1.158	0.125	2.153	0.211	-3.22%
					0.952	0.100	1.110	0.117	2.065	0.200	4.22%	

Fig. 6. Results of \mathcal{L}_{SVL} on cross-domain test set.

speakers. In this section, we explore the effectiveness of the proposed global-level uncertainty supervision.

1) *Effect of the Scale*: As far as we know, few studies have systematically examined the effect of the scale parameter in speaker recognition. In this section, we investigate the effect of the scale s and how varying its value influences the performance of the speaker recognition system. The default scale in AAM-Softmax is $s = 32$. Based on this setting, we examine how the performance changes when the scale is increased or decreased. Specifically, we design two additional experiments: (1) a linearly increasing schedule where the scale grows from 32 to 48, and (2) a linearly decreasing schedule where the scale drops from 32 to 16. As shown in Fig. 7, increasing the scale generally improves performance on the hard test set (Vox1-H), while yielding slightly worse results on the easier sets (Vox1-O and Vox1-E). This behavior arises because a larger scale sharpens the softmax distribution, causing the gradient to emphasize harder samples. In contrast, decreasing the scale consistently degrades performance across all test sets, indicating that a small scale severely harms discriminability.

2) *Ablation Study on the Bias Term Λ* : Table II reports the performance of our proposed uncertainty-aware AAM-Softmax ($\mathcal{L}_{\text{AAM}_u}$ Equation 19). Exp. 9 adopts a static constant Identity matrix as the bias term Λ , since the covariance matrix $\Sigma^s \geq 0$, the resulting uncertainty-aware scale s_u is always less than 1. Consequently, the final scale applied during training $s \cdot s_u$ is consistently reduced. According to our analysis in

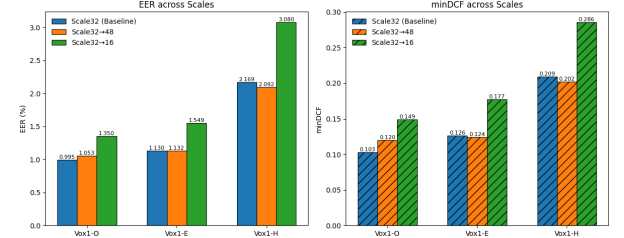


Fig. 7. Speaker verification performance under different scale settings.

Section VIII-C1, it is detrimental to performance. As expected, Exp. 9 fails to outperform the baseline.

Exp. 10 adopts dynamically varying Λ derived from $\Delta_{\cos} = (\cos \theta_{y_i} - \max_{j \neq y_i} \cos \theta_j) \cdot \text{detach}()$, i.e., the difference between the target cosine and the maximum non-target cosine, so that Δ_{\cos} is not influenced by parameter updates during training and is only used as a difficulty indicator. This term can be interpreted as a measure of how difficult a sample is to learn: a larger Δ_{\cos} implies that the sample is easier. Empirically, we find that most Δ_{\cos} values lie within the range of -0.8 to 0.5. We assume that Δ_{\cos} plays two important roles:

(1) *Training progression*: Δ_{\cos} tends to increase as training proceeds, which naturally drives the uncertainty scale s_u upward in later stages. This behavior aligns with our intuition in Section VIII-C1, that a larger scale is desirable.

(2) *Early-stage discrimination*: At the early stage of training, the estimated uncertainty Σ^s is neither accurate nor sufficiently discriminative across different samples. Incorporating Δ_{\cos} introduces sample-specific variation into s_u for different samples, providing a learning signal that helps the model form more meaningful uncertainty estimates.

Exp. 10 achieves slightly better performance than Exp. 9, demonstrating the benefit of integrating Δ_{\cos} . Exp. 12 further modifies the design by setting $\Lambda = 0.5 \mathbf{I} - \Delta_{\cos}$ ⁶. This reduces the constant component and increases the dynamic influence of Δ_{\cos} . As a result, Exp. 12 outperforms Exp. 10 in terms of average performance, particularly on the in-domain test sets.

To verify the necessity of modeling utterance-level uncertainty, we ablate the covariance term by removing Σ^s and retaining only Λ in Equation 16, as shown in Exp. 11. Compared with Exp. 10, this removal leads to a clear

⁶0.5 \mathbf{I} is the smallest constant we tested that prevents NaN issues during training while ensuring that Λ remains non-negative.

TABLE II
OVERALL RESULTS OF GLOBAL-LEVEL UNCERTAINTY SUPERVISION ON IN-DOMAIN AND CROSS-DOMAIN SETS.
 $\Delta_{\cos} = (\cos \theta_{y_i} - \max_{j \neq y_i} \cos \theta_j) \cdot \text{detach}()$ WHICH SERVES AS THE DIFFICULTY INDICATOR.

# Exp	Loss	Λ	Σ^s	In-domain Test				Avg. Δ	Cross-domain Test				Avg.
				Vox1-O EER minDCF	Vox1-E EER minDCF	Vox1-H EER minDCF	Avg. Δ		SITW-Dev EER minDCF	SITW-Eval EER minDCF	Avg. Δ		
2	\mathcal{L}_{AAM}	-	✓	0.995 0.103	1.130 0.126	2.169 0.209	Benchmark		2.079 0.180	2.357 0.175	Benchmark		
9	$\mathcal{L}_{\text{AAM}_u}$	\mathbf{I}	✓	1.090 0.120	1.159 0.125	2.188 0.209	-4.33% -5.28%		2.079 0.171	2.314 0.182	0.91% 0.79%		
10	$\mathcal{L}_{\text{AAM}_u}$	$\mathbf{I} - \Delta_{\cos}$	✓	1.010 0.108	1.120 0.126	2.107 0.205	0.74% -1.65%		2.199 0.171	1.998 0.181	4.73% 0.79%		
11	$\mathcal{L}_{\text{AAM}_u}$	$\mathbf{I} - \Delta_{\cos}$	✗	1.128 0.106	1.137 0.124	2.122 0.210	-3.94% -0.60%		2.128 0.178	2.433 0.183	-2.79% -1.73%		
12	$\mathcal{L}_{\text{AAM}_u}$	$0.5 \mathbf{I} - \Delta_{\cos}$	✓	0.995 0.107	1.087 0.120	1.957 0.196	4.53% 2.37%		2.050 0.158	2.214 0.177	3.73% 5.54%		

TABLE III
COMPARISON OF DIFFERENT ATTENTION VARIANTS FOR UNCERTAINTY ESTIMATION. ‘-4’ DENOTES THE USE OF A 4-HEAD ATTENTION CONFIGURATION. THE SPEAKER ENCODER ACROSS ALL EXPERIMENTS IS STILL ECAPA-TDNN.

Model	# Param. (M)	Flops (G)	In-domain Test						Cross-domain Test		Avg. Δ	
			VoxI-O			VoxI-E			SITW-Dev			
			EER / minDCF	EER / minDCF	EER / minDCF	EER / minDCF	EER / minDCF	EER / minDCF	EER / minDCF	EER / minDCF		
xi-vector [24]	5.90	1.04	0.995 / 0.103	1.130 / 0.126	2.169 / 0.209	2.079 / 0.180	2.357 / 0.175				Benchmark	
xi+MHA-4	6.69	1.20	1.016 / 0.122	1.170 / 0.133	2.223 / 0.219	2.079 / 0.177	2.264 / 0.182				-3.53%	
xi+MHA-8	6.69	1.20	1.048 / 0.116	1.145 / 0.128	2.117 / 0.207	1.733 / 0.165	1.941 / 0.181				2.17%	
xi+MHA-16	6.69	1.20	0.872 / 0.126	1.128 / 0.127	2.127 / 0.211	1.771 / 0.168	2.012 / 0.202				1.11%	
xi+MHA-32	6.69	1.20	1.032 / 0.145	1.127 / 0.126	2.122 / 0.217	1.810 / 0.164	1.919 / 0.171				-0.32%	
xi+MVA-8	6.69	1.20	1.010 / 0.107	1.123 / 0.128	2.121 / 0.206	1.617 / 0.159	1.867 / 0.170				5.48%	

performance drop, indicating that estimating utterance-level uncertainty is essential. This result indicates that the gains from global-level uncertainty supervision are not solely due to the dynamic scaling effect, but also arise from more accurate, sample-specific uncertainty estimation provided by Σ^s .

D. The Effectiveness of Temporal Modeling

In this section, we incorporate a Transformer encoder to model temporal dependencies and compare multi-head attention (MHA) with different head configurations, as reported in Table III. The results show that the 8-head configuration achieves the best performance among all MHA variants. Based on this setting, we further encourage each attention head to capture a distinct temporal context, forming our proposed multi-view self-attention (MVA) mechanism. Experimental results demonstrate that MVA further improves performance, yielding over a 5% relative gain while introducing only minimal additional parameters and computational overhead.

E. \mathcal{U}^3 -xi: Combining All Components

In this section, we integrate all proposed components into a unified model—including the global-level uncertainty supervision (\mathcal{L}_{AAM_u}), the multi-view self-attention based uncertainty estimation module, and the uncertainty-aware scoring mechanism—and evaluate the overall performance gain. This combined system, referred to as \mathcal{U}^3 -xi, allows us to examine the cumulative benefit and the interaction among these three complementary designs. Table IV presents the performance improvements obtained by progressively incorporating each component. To more clearly verify the effectiveness of the proposed uncertainty estimation, we use the original ECAPA-TDNN with attentive statistical temporal pooling (ASTP) [16] as the baseline.

We progressively add the proposed modules as follows:

(1) Replacing ASTP with a lightweight uncertainty estimation module: The original xi-vector [24] replaces ASTP with a two-layer Gaussian posterior inference module that estimates

frame-level uncertainty using two simple linear projections. This architectural change alone yields relative improvements of 6.53% in EER and 8.76% in minDCF, demonstrating the effectiveness of incorporating uncertainty estimation into the speaker embedding framework.

(2) Introducing multi-view self-attention (MVA) for temporal modeling: Building on the previous configuration, MVA-8 incorporates a Transformer encoder with MVA of 8 attention heads to enhance nonlinear modeling capacity and capture richer temporal dependencies. This addition yields further relative performance gains, demonstrating the effectiveness of strengthened temporal uncertainty modeling.

(3) Applying global-level uncertainty supervision: By inserting uncertainty into the scale of *softmax* function \mathcal{L}_{AAM_u} , the model receives explicit supervision to learn more reliable and discriminative uncertainty representations. This global guidance further enhances generalization across both in-domain and cross-domain conditions.

(4) Incorporating uncertainty scoring: We attempted to learn the scaling factor ρ using the SVL loss, as shown in Table I. However, this approach failed to converge, with NaN values occurring during training, indicating a conflict between \mathcal{L}_{SVL} and \mathcal{L}_{AAM_u} . Consequently, we fix $\rho = 1$ as a static scaling factor, which is also intuitively reasonable since the proposed global-level supervision already yields sufficiently discriminative uncertainty estimation. With uncertainty-aware scoring enabled, the final system achieves the largest performance improvement, obtaining relative gains of 21.1% and 15.57% over the baseline in terms of EER and minDCF, respectively.

F. Systematic Analysis of Uncertainty in the \mathcal{U}^3 -xi Model

1) *Relationship between Uncertainty and Sample Difficulty*: We first investigate the relationship between utterance-level uncertainty (i.e., the diagonal covariance Σ^s) and the cosine gap Δ_{\cos} , which serves as a measure of the classification difficulty of sample i , where a larger gap indicates that the sample is easier to classify. Fig. 9 compares this relationship before

TABLE IV
ABLATION STUDY OF PROGRESSIVELY INCORPORATING EACH COMPONENT IN THE PROPOSED \mathcal{U}^3 -XI MODEL. ECAPA-TDNN IS USED AS THE SPEAKER ENCODER IN ALL EXPERIMENTS.

Model	#Param.	In-domain Test						Cross-domain Test		Avg. Δ EER / minDCF	
		VoxI-O		VoxI-E		VoxI-H		SITW-Dev			
		EER / minDCF	EER / minDCF	EER / minDCF	EER / minDCF	EER / minDCF	EER / minDCF	EER / minDCF	EER / minDCF		
ASTP [16]	6.19 M	1.069 / 0.122	1.209 / 0.136	2.310 / 0.226	2.310 / 0.184	2.433 / 0.197				Benchmark	
xi [24]	5.90 M	0.995 / 0.103	1.130 / 0.126	2.169 / 0.209	2.079 / 0.180	2.357 / 0.175				6.53% / 8.76%	
\mathcal{U}^3 -xi	+MVA-8	6.69 M	1.010 / 0.107	1.123 / 0.128	2.121 / 0.206	1.617 / 0.159	1.867 / 0.170				14.81% / 10.86%
	+ \mathcal{L}_{AAM_u}	6.69 M	0.856 / 0.109	1.064 / 0.121	1.982 / 0.195	1.854 / 0.162	2.105 / 0.170				15.85% / 12.22%
	+ $\rho = 1$	6.69 M	0.782 / 0.100	1.016 / 0.115	1.888 / 0.187	1.770 / 0.160	1.921 / 0.169				21.10% / 15.57%

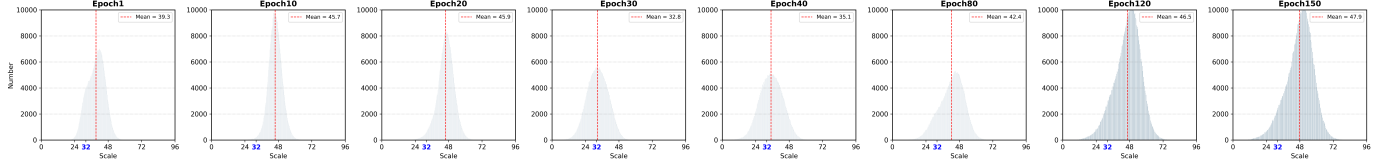


Fig. 8. Distribution of the sample-wise scale across training epochs. The x-axis represents the scale values, and the y-axis represents the number of samples corresponding to each scale value. The blue number 32 is the default scale.

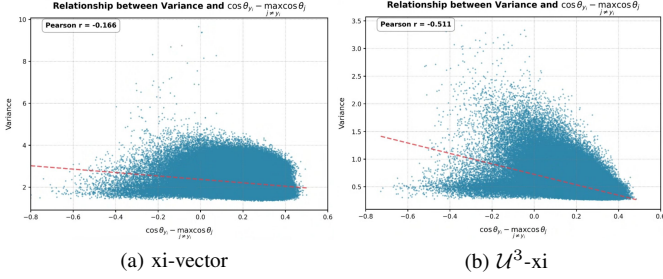


Fig. 9. Relationship between utterance-level variance and sample difficulty on the training set. The y-axis shows the averaged diagonal variance across all embedding dimensions.

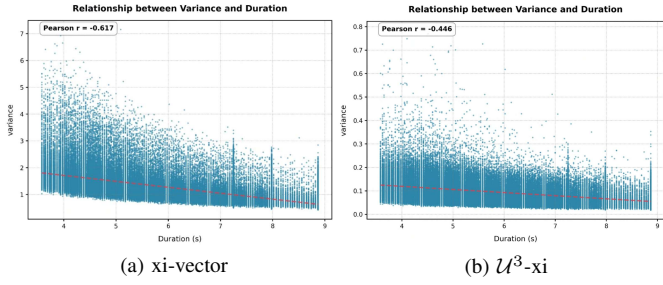


Fig. 10. Relationship between utterance-level variance and its duration on the Vox1 test set, including Vox1-O, Vox1-E and Vox1-H.

and after applying our proposed method $\mathcal{U}^3\text{-xi}$. The Pearson correlation coefficient decreases from -0.166 (xi-vector) to -0.511 ($\mathcal{U}^3\text{-xi}$), demonstrating that the proposed method strengthens the negative correlation between uncertainty and sample easiness. This trend indicates that $\mathcal{U}^3\text{-xi}$ produces more discriminative and interpretable uncertainty, assigning lower variance to easier samples and higher variance to harder ones. This demonstrates that our global-level uncertainty supervision indeed provides meaningful and effective guidance.

2) *Relationship between Uncertainty and Sample Duration:* Fig. 10 illustrates the relationship between utterance-level uncertainty and utterance duration on the test set, since all training samples are truncated to 2 seconds. Both subfigures show a clear trend that longer utterances tend to have lower estimated variance, which aligns with the intuitive understanding that embeddings extracted from longer speech segments are generally more robust. Interestingly, we observe that this correlation appears weaker for our proposed $\mathcal{U}^3\text{-xi}$ model. Despite this weaker dependency on utterance duration, $\mathcal{U}^3\text{-xi}$ still outperforms the baseline xi-vector model. One possible explanation is that $\mathcal{U}^3\text{-xi}$ may capture aspects of utterance quality beyond length, allowing it to assign lower uncertainty even to short but high-quality utterances.

3) *The Distribution of Sample-wise Scale Across Training Epochs:* Fig. 7 suggests that using a slightly larger scale may benefit optimization. In this section, we further investigate this phenomenon by visualizing how the sample-wise scale

evolves across training epochs. Our method predicts a sample-dependent scale, meaning that each utterance is assigned a single scale value during training. For each epoch, we count the number of samples that fall into each scale value and summarize the statistics in Fig. 8. Several observations can be made: 1. In each epoch, some samples receive scales smaller than 32, while others receive scales larger than 32. This indicates that the model adaptively assigns different scales according to sample difficulty. 2. Before the margin starts increasing ($\text{epoch} \leq 20$), the mean scale gradually rises. Once the margin begins increasing ($20 < \text{epoch} \leq 40$), the mean scale drops significantly. After the margin is fixed ($\text{epoch} > 40$), the mean scale gradually increases again. This behavior reflects the sensitivity of the scale to changes in the angular margin. At the start of training, the model focuses on easier samples, as smaller scales soften the softmax distribution and cause the gradient to emphasize these samples. As training progresses, the scale gradually increases, shifting the model's attention toward harder samples. In summary, a dynamic scale plays a crucial role in balancing the contribution of each training utterance. Moreover, the progressively right-shifting scale distribution resembles a curriculum learning strategy [69], guiding the model to focus on easier samples first and gradually adapt to harder ones.

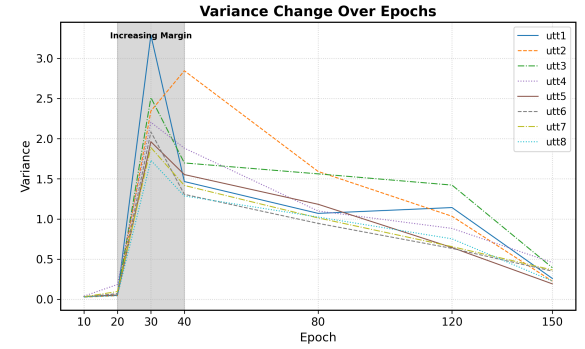


Fig. 11. Uncertainty score (Variance) of different utterances changes during training epochs. The margin is linearly increasing during epoch 20 to 40. The y-axis shows the averaged diagonal variance across all embedding dimensions

4) *Uncertainty Dynamics during Training:* From Fig. 11, we observe that the uncertainty values are very small at the early stages of training, and then gradually increase. When the margin starts to increase (epoch 20–40), the uncertainty variance also rises significantly, indicating that the uncertainty estimation module is highly sensitive to changes in the margin. After the margin is fixed, the uncertainty scores gradually decrease as training progresses, which suggests that the network becomes more stable and converges toward a

⁷† indicates that these results are directly inferred using the pretrained WeSpeaker model available at <https://github.com/wenet-e2e/wespeaker/blob/master/docs/pretrained.md>. [‡] means we retrain these models by ourselves.

more confident embedding space. This observation implies that, although we aim to model data uncertainty rather than model uncertainty, the estimated uncertainty is still influenced by the optimization status of the model. In addition, the relative uncertainty across different utterances is not consistent throughout training. For example, the uncertainty score of utterance 2 is the highest around epoch 40 but later becomes lower than that of other utterances. This behavior indicates that the uncertainty estimation is not immediately accurate at the beginning of training; rather, it dynamically adjusts and becomes more reliable as training progresses. Overall, no obvious global pattern is observed across all utterances.

G. Generalization Ability to Other Speaker Encoders

Table V presents a comparison between our methods and other state-of-the-art approaches. The results demonstrate that our method achieves competitive, and in some cases superior, performance while using fewer parameters.

1) *In-domain Test*: Considering ECAPA-TDNN512 (Rows 8–10), ResNet34 (Rows 11–13), and ReDimNet-B2 (Rows 14, 18, and 19), we observe that the proposed \mathcal{U}^3 -xi consistently achieves performance improvements over their corresponding baselines. Furthermore, applying uncertainty-aware scoring with $\rho = 1$ generally leads to additional gains. The only exceptions are ReDimNet-B2 evaluated on Vox1-E and Vox1-H, where minDCF slightly increases from 0.089 to 0.091 and from 0.153 to 0.157, respectively.

In terms of average performance, the relative improvements are 18.65% for ECAPA-TDNN512, 13.29% for ResNet34, and

9.45% for ReDimNet-B2. These results indicate that while \mathcal{U}^3 -xi remains effective across different speaker encoders, the margin for improvement diminishes as the underlying encoder becomes more advanced.

2) *Cross-domain Test*: The SITW-EVAL set is relatively similar to VoxCeleb in terms of recording conditions; consequently, performance on this dataset follows trends similar to those observed in the in-domain evaluation. Specifically, \mathcal{U}^3 -xi delivers consistent improvements across different speaker encoders, while uncertainty-aware scoring leads to a slight degradation in terms of minDCF.

In contrast, on the more challenging cross-domain CVCeleb dataset, the proposed method improves EER but fails to yield consistent gains in minDCF. Even after applying uncertainty-aware scoring, minDCF further degrades in several cases, with extreme failures observed for Rows 10 and 18, where minDCF spikes to 1.0, clearly indicating invalid result. To further investigate this issue, we plot the Detection Error Tradeoff (DET) curves for Rows 9 and 10, as shown in Fig. 12. It can be observed that the DET curve of Row 10 becomes severely distorted. Compared with the relatively smooth and well-balanced curve of Row 9, the curve of Row 10 exhibits a much steeper and less stable tradeoff between the false-alarm rate (FAR) and the false-reject rate (FRR).

This distortion suggests that uncertainty-aware scoring, while optimizing EER (i.e., the operating point where FAR and FRR are equal), fails to preserve a stable tradeoff across a broader range of operating points. As a result, this imbalance directly leads to erratic minDCF behavior, including the

TABLE V

PERFORMANCE COMPARISON ACROSS DIFFERENT SPEAKER ENCODERS. CELLS HIGHLIGHTED IN GRAY INDICATE THE APPLICATION OF THE PROPOSED METHODS. ‘LM’ DENOTES LARGE-MARGIN FINE-TUNING. ‘AS-NORM’ DENOTES ADAPTIVE S-NORM [70]. ‘QMF’ REFERS TO THE QUALITY MEASURE FUNCTION [71]. RESULTS SHOWN IN GRAY CORRESPOND TO THE PROPOSED METHODS. $\rho = 1$ MEANS WE APPLY UNCERTAINTY-AWARE COSINE SCORING.

Row	Speaker ⁷ Encoder	# Param. (M)	LM	AS- Norm (M)	Q M	In-domain Test			Cross-domain Test		Avg. Δ In Cross
						Vox1-O F	EER / minDCF FEER / minDCF	Vox1-H EER / minDCF FEER / minDCF	SITW-Eval EER / minDCF	CNCeleb FEER / minDCF	
1	ECAPA-TDNN1024 [51]	14.65	✗	✓	✓	0.660 / 0.078	0.882 / 0.094	1.606 / 0.159	-	-	-
2	ConFusionformer-9 [62]	10.9	✗	✓	✗	0.68 / 0.064	0.93 / 0.104	1.66 / 0.166	-	-	-
3	CAM++ [†] [72]	7.2	✗	✗	✗	0.808 / 0.109	0.931 / 0.109	1.863 / 0.179	1.704 / 0.166	15.179 / 0.635	-
4	Gemini SD-ResNet38 [73]	6.72	✗	✗	✗	1.085 / 0.099	1.130 / 0.117	1.974 / 0.185	1.523 / 0.147	11.507 / 0.553	-
5	Gemini DF-ResNet114 [†] [73]	6.53	✓	✗	✗	0.771 / 0.065	0.906 / 0.097	1.599 / 0.156	1.603 / 0.121	10.960 / 0.504	-
6	RecXi with L_{ssp} [27]	7.06	✗	✗	✗	0.984 / 0.091	1.075 / 0.114	1.857 / 0.179	1.340 / 0.137	-	-
7	ECAPA-TDNN1024 [16] [†]	14.65	✗	✗	✗	0.856 / 0.090	1.072 / 0.117	2.059 / 0.205	2.269 / 0.174	15.532 / 0.670	-
8	ECAPA-TDNN512 [16] [†]	6.19	✗	✗	✗	1.069 / 0.122	1.209 / 0.136	2.310 / 0.226	2.433 / 0.197	15.314 / 0.633	Benchmark
9	+ \mathcal{U}^3 -xi ($\rho = 0$)		✗	✗	✗	0.856 / 0.109	1.064 / 0.121	1.982 / 0.195	2.105 / 0.170	13.706 / 0.608	13.57% 10.41%
10	+ \mathcal{U}^3 -xi ($\rho = 1$)		✗	✗	✗	0.782 / 0.100	1.016 / 0.115	1.888 / 0.187	1.921 / 0.169	10.271 / 1.000	18.64% 2.54%
11	ResNet34 [74] [†]	6.63	✗	✗	✗	0.867 / 0.091	1.049 / 0.121	1.960 / 0.192	1.903 / 0.159	11.090 / 0.488	Benchmark
12	+ \mathcal{U}^3 -xi ($\rho = 0$)		✗	✗	✗	0.888 / 0.085	0.900 / 0.099	1.712 / 0.175	1.435 / 0.135	11.732 / 0.513	9.59% 7.19%
13	+ \mathcal{U}^3 -xi ($\rho = 1$)		✗	✗	✗	0.867 / 0.078	0.868 / 0.095	1.641 / 0.172	1.367 / 0.134	10.082 / 0.541	13.29% 10.53%
14			✗	✗	✗	0.782 / 0.064	0.907 / 0.097	1.667 / 0.162	1.558 / 0.148	12.385 / 0.552	Benchmark
15			✓	✗	✗	0.750 / 0.072	0.868 / 0.093	1.560 / 0.147	1.293 / 0.120	12.509 / 0.565	2.47% 8.14%
16	ReDimNet-B2 [‡] [75]	4.89	✓	✓	✗	0.675 / 0.063	0.826 / 0.088	1.437 / 0.135	1.213 / 0.154	10.662 / 0.518	10.66% 9.55%
17			✓	✓	✓	0.686 / 0.060	0.805 / 0.084	1.395 / 0.130	1.176 / 0.155	9.254 / 0.585	13.21% 9.77%
18	+ \mathcal{U}^3 -xi ($\rho = 0$)		✗	✗	✗	0.649 / 0.073	0.801 / 0.089	1.532 / 0.153	1.422 / 0.127	13.464 / 0.552	5.76% 3.55%
19	+ \mathcal{U}^3 -xi ($\rho = 1$)		✗	✗	✗	0.606 / 0.065	0.779 / 0.091	1.494 / 0.157	1.394 / 0.141	9.479 / 1.000	9.45% -10.63%
20	+ $\bar{\mathcal{U}}^3$ -xi ($\rho = 0$)					0.670 / 0.070	0.770 / 0.081	1.437 / 0.144	1.230 / 0.098	12.877 / 0.622	10.88% 9.04%
21	+ $\bar{\mathcal{U}}^3$ -xi ($\rho = 1$)					0.489 / 0.076	0.698 / 0.104	1.311 / 0.203	1.017 / 0.211	10.267 / 1.000	1.60% -13.45%
22	+ $\bar{\mathcal{U}}^3$ -xi ($\rho = 0$)					0.622 / 0.069	0.726 / 0.074	1.327 / 0.126	1.093 / 0.125	11.462 / 0.740	16.47% 4.70%
23	+ $\bar{\mathcal{U}}^3$ -xi ($\rho = 1$)					0.399 / 0.080	0.638 / 0.089	1.170 / 0.171	0.875 / 0.224	9.738 / 1.000	16.22% -16.58%
24	+ $\bar{\mathcal{U}}^3$ -xi ($\rho = 0$)					0.596 / 0.070	0.705 / 0.071	1.298 / 0.124	0.875 / 0.227	10.115 / 0.832	18.18% -10.48%
25	+ $\bar{\mathcal{U}}^3$ -xi ($\rho = 1$)					0.569 / 0.064	0.679 / 0.068	1.234 / 0.121	1.066 / 0.131	10.436 / 1.000	22.26% -5.59%

extreme values observed on CNCeleb.

We hypothesize that this limitation arises from poor generalization of the uncertainty estimation mechanism to cross-domain conditions. During training on VoxCeleb2, variations in recording conditions may be implicitly modeled as a form of uncertainty. However, in cross-domain scenarios such as CNCeleb, the acoustic conditions differ substantially from those seen during training, causing the uncertainty estimator to fail in producing accurate or meaningful uncertainty estimates.

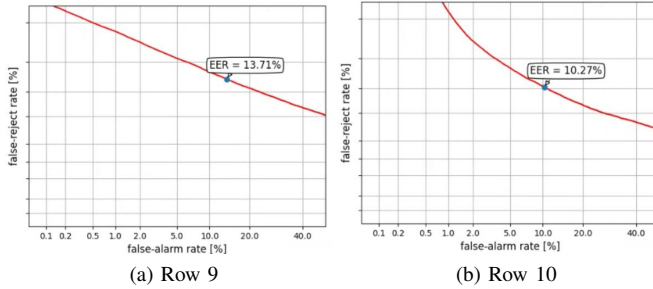


Fig. 12. The Detection Error Tradeoff (DET) curve on CNCeleb dataset.

3) *The effect of LM, AS-Norm and QMF on Uncertainty:* We further explore the compatibility of our \mathcal{U}^3 -xi framework with commonly used training-time fine-tuning and backend score processing methods, including LM fine-tuning, AS-Norm, and QMF (Rows 15-17, 20-25 in Table V). Overall, these techniques are compatible with \mathcal{U}^3 -xi and can provide additional performance gains when applied jointly.

Considering the large-margin (LM) setting (Rows 15, 20, and 21), these results illustrate the performance changes after large-margin fine-tuning. Consistent with previous findings, our method improves EER across most test sets, except for Row 20 on CNCeleb. In contrast, while minDCF improves on in-domain and SITW-Eval, it fails on the more challenging cross-domain CNCeleb dataset. Furthermore, after applying uncertainty-aware cosine scoring (Row 21), EER remains improved, whereas minDCF consistently degrades across all test sets.

Considering AS-Norm (Rows 16, 22, and 23), similar trends are observed as with the LM setting: our method performs well on in-domain EER, but shows limited effectiveness on cross-domain data. In addition, uncertainty-aware cosine scoring fails to improve minDCF in both in-domain and cross-domain scenarios.

QMF alleviates these issues to some extent, as seen by comparing Rows 17, 24, and 25. Both Rows 24 and 25 outperform Row 17 on in-domain data in most cases. However, for cross-domain data, the method still fails to achieve improvements.

IX. CONCLUSION AND LIMITATIONS

We investigate the incorporation of uncertainty into speaker recognition systems and propose two uncertainty supervision strategies, together with a redesigned uncertainty estimation module. By integrating these components into a unified framework, termed \mathcal{U}^3 -xi, we observe consistent and substantial performance improvements across multiple experimental settings. These results suggest that explicitly modeling uncertainty is a promising direction for advancing speaker recognition performance. Nevertheless, several limitations remain.

In particular, uncertainty-aware scoring does not consistently improve minDCF, especially on cross-domain evaluation sets. This indicates that the uncertainty estimation for cross-domain data may not accurate enough. In future work, we plan to investigate more robust uncertainty estimation methods and examine the scalability of the proposed framework to large-scale training datasets.

X. ACKNOWLEDGMENTS

I would like to thank Jinghan Liu, Tianchi Liu, and Yi Ma for their excellent work and kind assistance, which has provided substantial inspiration for completing this paper.

REFERENCES

- [1] J. A. Markowitz, "Voice biometrics," *Communications of the ACM*, vol. 43, no. 9, pp. 66–73, 2000.
- [2] S. Wang, Z. Chen, K. A. Lee, Y. Qian, and H. Li, "Overview of speaker modeling and its applications: From the lens of deep speaker representation learning," *IEEE/ACM Transactions on Audio, Speech, and Language Processing*, 2024.
- [3] I. McGraw, R. Prabhavalkar, R. Alvarez, M. G. Arenas, K. Rao, D. Rybach, O. Alsharif, H. Sak, A. Gruenstein, F. Beaufays *et al.*, "Personalized speech recognition on mobile devices," in *2016 IEEE International Conference on Acoustics, Speech and Signal Processing (ICASSP)*. IEEE, 2016, pp. 5955–5959.
- [4] E. Kiktova and J. Juhar, "Speaker recognition for surveillance application," *Journal of Electrical and Electronics Engineering*, vol. 8, no. 2, p. 19, 2015.
- [5] J. Li, K. Zhang, S. Wang, H. Li, M.-W. Mak, and K. A. Lee, "On the effectiveness of enrollment speech augmentation for target speaker extraction," in *2024 IEEE Spoken Language Technology Workshop (SLT)*. IEEE, 2024, pp. 325–332.
- [6] Z. Du, Q. Chen, S. Zhang, K. Hu, H. Lu, Y. Yang, H. Hu, S. Zheng, Y. Gu, Z. Ma *et al.*, "Cosyvoice: A scalable multilingual zero-shot text-to-speech synthesizer based on supervised semantic tokens," *arXiv preprint arXiv:2407.05407*, 2024.
- [7] H. Lu, Z. Wu, D. Dai, R. Li, S. Kang, J. Jia, and H. Meng, "One-shot voice conversion with global speaker embeddings," in *Interspeech*, 2019, pp. 669–673.
- [8] C. Li, X. Ma, B. Jiang, X. Li, X. Zhang, X. Liu, Y. Cao, A. Kannan, and Z. Zhu, "Deep speaker: an end-to-end neural speaker embedding system," *arXiv preprint arXiv:1705.02304*, 2017.
- [9] D. Snyder, D. Garcia-Romero, G. Sell, D. Povey, and S. Khudanpur, "X-vectors: Robust dnn embeddings for speaker recognition," in *2018 IEEE international conference on acoustics, speech and signal processing (ICASSP)*. IEEE, 2018, pp. 5329–5333.
- [10] S. Wang, Y. Yang, Y. Qian, and K. Yu, "Revisiting the statistics pooling layer in deep speaker embedding learning," in *2021 12th International Symposium on Chinese Spoken Language Processing (ISCSLP)*. IEEE, 2021, pp. 1–5.
- [11] K. Okabe, T. Koshinaka, and K. Shinoda, "Attentive statistics pooling for deep speaker embedding," in *Interspeech 2018*, 2018, pp. 2252–2256.
- [12] Y. Zhu, T. Ko, D. Snyder, B. Mak, and D. Povey, "Self-attentive speaker embeddings for text-independent speaker verification," in *Interspeech*, vol. 2018, 2018, pp. 2–6.
- [13] M. India, P. Safari, and J. Hernando, "Self multi-head attention for speaker recognition," in *Interspeech 2019*, 2019, pp. 4305–4309.
- [14] M. Zhao, Y. Ma, Y. Ding, Y. Zheng, M. Liu, and M. Xu, "Multi-query multi-head attention pooling and inter-topk penalty for speaker verification," in *ICASSP 2022-2022 IEEE International Conference on Acoustics, Speech and Signal Processing (ICASSP)*. IEEE, 2022, pp. 6737–6741.
- [15] Y. Wu, C. Guo, H. Gao, X. Hou, and J. Xu, "Vector-based attentive pooling for text-independent speaker verification," in *Interspeech*, 2020, pp. 936–940.
- [16] B. Desplanques, J. Thienpondt, and K. Demuynck, "Ecapa-tdnn: Emphasized channel attention, propagation and aggregation in tdnn based speaker verification," in *Interspeech 2020*, 2020, pp. 3830–3834.
- [17] Y. Ma, S. Wang, T. Liu, and H. Li, "Expo: Explainable phonetic trait-oriented network for speaker verification," *IEEE Signal Processing Letters*, 2025.

- [18] J. Chang, Z. Lan, C. Cheng, and Y. Wei, "Data uncertainty learning in face recognition," in *Proceedings of the IEEE/CVF conference on computer vision and pattern recognition*, 2020, pp. 5710–5719.
- [19] F.-Z. Ou, X. Chen, R. Zhang, Y. Huang, S. Li, J. Li, Y. Li, L. Cao, and Y.-G. Wang, "Sdd-fqua: Unsupervised face image quality assessment with similarity distribution distance," in *Proceedings of the IEEE/CVF conference on computer vision and pattern recognition*, 2021, pp. 7670–7679.
- [20] Y. Shi and A. K. Jain, "Probabilistic face embeddings," in *Proceedings of the IEEE/CVF international conference on computer vision*, 2019, pp. 6902–6911.
- [21] Y. Ji, J. Wang, Y. Gong, L. Zhang, Y. Zhu, H. Wang, J. Zhang, T. Sakai, and Y. Yang, "Map: Multimodal uncertainty-aware vision-language pre-training model," in *Proceedings of the IEEE/CVF conference on computer vision and pattern recognition*, 2023, pp. 23 262–23 271.
- [22] Q. Meng, S. Zhao, Z. Huang, and F. Zhou, "Magface: A universal representation for face recognition and quality assessment," in *Proceedings of the IEEE/CVF conference on computer vision and pattern recognition*, 2021, pp. 14 225–14 234.
- [23] K. Chen, T. Yi, and Q. Lv, "Fast and reliable probabilistic face embeddings based on constrained data uncertainty estimation," *Image and Vision Computing*, vol. 121, p. 104429, 2022.
- [24] K. A. Lee, Q. Wang, and T. Koshinaka, "Xi-vector embedding for speaker recognition," *IEEE Signal Processing Letters*, vol. 28, pp. 1385–1389, 2021.
- [25] D. A. Reynolds, T. F. Quatieri, and R. B. Dunn, "Speaker verification using adapted gaussian mixture models," *Digital signal processing*, vol. 10, no. 1-3, pp. 19–41, 2000.
- [26] N. Dehak, P. J. Kenny, R. Dehak, P. Dumouchel, and P. Ouellet, "Front-end factor analysis for speaker verification," *IEEE Transactions on Audio, Speech, and Language Processing*, vol. 19, no. 4, pp. 788–798, 2010.
- [27] T. Liu, K. A. Lee, Q. Wang, and H. Li, "Disentangling voice and content with self-supervision for speaker recognition," *Advances in Neural Information Processing Systems*, vol. 36, pp. 50 221–50 236, 2023.
- [28] R. Wang, L. Chen, K. A. Lee, and Z.-H. Ling, "Asynchronous Voice Anonymization Using Adversarial Perturbation On Speaker Embedding," in *Interspeech 2024*, 2024, pp. 4443–4447.
- [29] L. Chen, K. A. Lee, W. Guo, and Z.-H. Ling, "Modeling pseudo-speaker uncertainty in voice anonymization," in *ICASSP 2024-2024 IEEE International Conference on Acoustics, Speech and Signal Processing (ICASSP)*. IEEE, 2024, pp. 11 601–11 605.
- [30] L. Chen, W. Gu, K. A. Lee, W. Guo, and Z.-H. Ling, "Pseudo-speaker distribution learning in voice anonymization," *IEEE/ACM Transactions on Audio, Speech, and Language Processing*, 2024.
- [31] A. Vaswani, N. Shazeer, N. Parmar, J. Uszkoreit, L. Jones, A. N. Gomez, Ł. Kaiser, and I. Polosukhin, "Attention is all you need," *Advances in neural information processing systems*, vol. 30, 2017.
- [32] R. Wang, J. Ao, L. Zhou, S. Liu, Z. Wei, T. Ko, Q. Li, and Y. Zhang, "Multi-view self-attention based transformer for speaker recognition," in *ICASSP 2022-2022 IEEE international conference on acoustics, speech and signal processing (ICASSP)*. IEEE, 2022, pp. 6732–6736.
- [33] A. Der Kiureghian and O. Ditlevsen, "Aleatory or epistemic? does it matter?" *Structural safety*, vol. 31, no. 2, pp. 105–112, 2009.
- [34] J. Mukhoti, A. Kirsch, J. Van Amersfoort, P. Torr, and Y. Gal, "Deterministic neural networks with inductive biases capture epistemic and aleatoric uncertainty," *arXiv preprint arXiv:2102.11582*, vol. 2, 2021.
- [35] J. Mukhoti, A. Kirsch, J. Van Amersfoort, P. H. Torr, and Y. Gal, "Deep deterministic uncertainty: A new simple baseline," in *Proceedings of the IEEE/CVF Conference on Computer Vision and Pattern Recognition*, 2023, pp. 24 384–24 394.
- [36] J. Li, K. A. Lee, D.-T. Truong, T. Liu, and M.-W. Mak, "Xi+: Uncertainty supervision for robust speaker embedding," *arXiv preprint arXiv:2509.05993*, 2025.
- [37] Q. Wang, K. A. Lee, and T. Liu, "Incorporating uncertainty from speaker embedding estimation to speaker verification," in *ICASSP 2023-2023 IEEE International Conference on Acoustics, Speech and Signal Processing (ICASSP)*. IEEE, 2023, pp. 1–5.
- [38] Q. Wang and K. A. Lee, "Cosine scoring with uncertainty for neural speaker embedding," *IEEE Signal Processing Letters*, 2024.
- [39] S. Barahona, A. Silnova, L. Mošner, J. Peng, O. Plchot, J. Rohdin, L. Zhang, J. Han, P. Palka, F. Landini *et al.*, "Analysis of abc frontend audio systems for the nist-sre24," *arXiv preprint arXiv:2505.15320*, 2025.
- [40] W. Liu, Y. Wen, Z. Yu, and M. Yang, "Large-margin softmax loss for convolutional neural networks," in *Proceedings of the 33rd International Conference on International Conference on Machine Learning-Volume 48*, 2016, pp. 507–516.
- [41] W. Liu, Y. Wen, Z. Yu, M. Li, B. Raj, and L. Song, "Sphereface: Deep hypersphere embedding for face recognition," in *Proceedings of the IEEE conference on computer vision and pattern recognition*, 2017, pp. 212–220.
- [42] H. Wang, Y. Wang, Z. Zhou, X. Ji, D. Gong, J. Zhou, Z. Li, and W. Liu, "Cosface: Large margin cosine loss for deep face recognition," in *Proceedings of the IEEE conference on computer vision and pattern recognition*, 2018, pp. 5265–5274.
- [43] J. Deng, J. Guo, N. Xue, and S. Zafeiriou, "Arcface: Additive angular margin loss for deep face recognition," in *Proceedings of the IEEE/CVF conference on computer vision and pattern recognition*, 2019, pp. 4690–4699.
- [44] X. Wang, S. Zhang, S. Wang, T. Fu, H. Shi, and T. Mei, "Mis-classified vector guided softmax loss for face recognition," in *Proceedings of the AAAI conference on artificial intelligence*, vol. 34, no. 07, 2020, pp. 12 241–12 248.
- [45] Y. Huang, Y. Wang, Y. Tai, X. Liu, P. Shen, S. Li, J. Li, and F. Huang, "Curricularface: adaptive curriculum learning loss for deep face recognition," in *proceedings of the IEEE/CVF conference on computer vision and pattern recognition*, 2020, pp. 5901–5910.
- [46] M. Kim, A. K. Jain, and X. Liu, "Adaface: Quality adaptive margin for face recognition," in *Proceedings of the IEEE/CVF conference on computer vision and pattern recognition*, 2022, pp. 18 750–18 759.
- [47] D. Zhou, L. Wang, K. A. Lee, Y. Wu, M. Liu, J. Dang, and J. Wei, "Dynamic margin softmax loss for speaker verification," in *INTERSPEECH*, 2020, pp. 3800–3804.
- [48] Y. Li, F. Gao, Z. Ou, and J. Sun, "Angular softmax loss for end-to-end speaker verification," in *2018 11th International Symposium on Chinese Spoken Language Processing (ISCSLP)*. IEEE, 2018, pp. 190–194.
- [49] Y. Liu, L. He, and J. Liu, "Large margin softmax loss for speaker verification," in *Proc. Interspeech 2019*, 2019, pp. 2873–2877.
- [50] L. Li, R. Nai, and D. Wang, "Real additive margin softmax for speaker verification," in *ICASSP 2022-2022 IEEE International Conference on Acoustics, Speech and Signal Processing (ICASSP)*. IEEE, 2022, pp. 7527–7531.
- [51] J. Liu, X. Wang, and J. Meng, "Adaspeaker: Learning discriminative speaker representations with gradient-aware adaptive scaling," in *Proceedings of the 33rd ACM International Conference on Multimedia*, 2025, pp. 660–668.
- [52] L. Shang, M. Huang, W. Shi, Y. Liu, Y. Liu, W. Steven, B. Sun, X. Xie, and Y. Qiao, "Improving training and inference of face recognition models via random temperature scaling," in *Proceedings of the AAAI conference on artificial intelligence*, vol. 37, no. 12, 2023, pp. 15 082–15 090.
- [53] H. Xuan, B. Yang, and X. Li, "Exploring the impact of temperature scaling in softmax for classification and adversarial robustness," *arXiv preprint arXiv:2502.20604*, 2025.
- [54] X. Zhang, R. Zhao, Y. Qiao, X. Wang, and H. Li, "Adacos: Adaptively scaling cosine logits for effectively learning deep face representations," in *Proceedings of the IEEE/CVF Conference on Computer Vision and Pattern Recognition*, 2019, pp. 10 823–10 832.
- [55] Y. Zhu, X. Gao, B. Ke, R. Qiao, and X. Sun, "Coarse-to-fine: Learning compact discriminative representation for single-stage image retrieval," in *Proceedings of the IEEE/CVF International Conference on Computer Vision*, 2023, pp. 11 260–11 269.
- [56] R. Kail, K. Fedyanin, N. Muravev, A. Zaytsev, and M. Panov, "Scaleface: Uncertainty-aware deep metric learning," in *2023 IEEE 10th International Conference on Data Science and Advanced Analytics (DSAA)*. IEEE, 2023, pp. 1–10.
- [57] Z. Bai and X.-L. Zhang, "Speaker recognition based on deep learning: An overview," *Neural Networks*, vol. 140, pp. 65–99, 2021.
- [58] H. Wang, C. Liang, S. Wang, Z. Chen, B. Zhang, X. Xiang, Y. Deng, and Y. Qian, "Wespeaker: A research and production oriented speaker embedding learning toolkit," in *ICASSP 2023-2023 IEEE International Conference on Acoustics, Speech and Signal Processing (ICASSP)*. IEEE, 2023, pp. 1–5.
- [59] S. Wang, Z. Chen, B. Han, H. Wang, C. Liang, B. Zhang, X. Xiang, W. Ding, J. Rohdin, A. Silnova *et al.*, "Advancing speaker embedding learning: Wespeaker toolkit for research and production," *Speech Communication*, vol. 162, p. 103104, 2024.
- [60] M. Sang, Y. Zhao, G. Liu, J. H. Hansen, and J. Wu, "Improving transformer-based networks with locality for automatic speaker verification," in *ICASSP 2023-2023 IEEE International Conference on Acoustics, Speech and Signal Processing (ICASSP)*. IEEE, 2023, pp. 1–5.

- [61] B. Han, Z. Chen, and Y. Qian, “Local information modeling with self-attention for speaker verification,” in *ICASSP 2022-2022 IEEE International Conference on Acoustics, Speech and Signal Processing (ICASSP)*. IEEE, 2022, pp. 6727–6731.
- [62] Y. Tu, M.-W. Mak, K.-A. Lee, and W. Lin, “Confusionformer: Locality-enhanced conformer through multi-resolution attention fusion for speaker verification,” *Neurocomputing*, p. 130429, 2025.
- [63] J. S. Chung, A. Nagrani, and A. Zisserman, “Voxceleb2: Deep speaker recognition,” *arXiv preprint arXiv:1806.05622*, 2018.
- [64] A. Nagrani, J. S. Chung, and A. Zisserman, “Voxceleb: a large-scale speaker identification dataset,” *arXiv preprint arXiv:1706.08612*, 2017.
- [65] M. McLaren, L. Ferrer, D. Castan, and A. Lawson, “The speakers in the wild (sitw) speaker recognition database,” in *Interspeech*, 2016, pp. 818–822.
- [66] Y. Fan, J. Kang, L. Li, K. Li, H. Chen, S. Cheng, P. Zhang, Z. Zhou, Y. Cai, and D. Wang, “Cn-celeb: a challenging chinese speaker recognition dataset,” in *ICASSP 2020-2020 IEEE International Conference on Acoustics, Speech and Signal Processing (ICASSP)*. IEEE, 2020, pp. 7604–7608.
- [67] D. Snyder, G. Chen, and D. Povey, “Musan: A music, speech, and noise corpus,” *arXiv preprint arXiv:1510.08484*, 2015.
- [68] T. Ko, V. Peddinti, D. Povey, M. L. Seltzer, and S. Khudanpur, “A study on data augmentation of reverberant speech for robust speech recognition,” in *2017 IEEE international conference on acoustics, speech and signal processing (ICASSP)*. IEEE, 2017, pp. 5220–5224.
- [69] P. Soviany, R. T. Ionescu, P. Rota, and N. Sebe, “Curriculum learning: A survey,” *International Journal of Computer Vision*, vol. 130, no. 6, pp. 1526–1565, 2022.
- [70] S. Cumani, P. D. Batzu, D. Colibro, C. Vair, P. Laface, and V. Vasilakakis, “Comparison of speaker recognition approaches for real applications,” in *Interspeech 2011*, 2011, pp. 2365–2368.
- [71] J. Thienpondt, B. Desplanques, and K. Demuynck, “The idlab voxsrc-20 submission: Large margin fine-tuning and quality-aware score calibration in dnn based speaker verification,” in *ICASSP 2021-2021 IEEE International Conference on Acoustics, Speech and Signal Processing (ICASSP)*. IEEE, 2021, pp. 5814–5818.
- [72] H. Wang, S. Zheng, Y. Chen, L. Cheng, and Q. Chen, “Cam++: A fast and efficient network for speaker verification using context-aware masking,” in *Proc. Interspeech 2023*, 2023, pp. 5301–5305.
- [73] T. Liu, K. A. Lee, Q. Wang, and H. Li, “Golden gemini is all you need: Finding the sweet spots for speaker verification,” *IEEE/ACM Transactions on Audio, Speech, and Language Processing*, vol. 32, pp. 2324–2337, 2024.
- [74] H. Zeinali, S. Wang, A. Silnova, P. Matějka, and O. Plchot, “But system description to voxceleb speaker recognition challenge 2019,” *arXiv preprint arXiv:1910.12592*, 2019.
- [75] I. Yakovlev, R. Makarov, A. Balykin, P. Malov, A. Okhotnikov, and N. Torgashov, “Reshape Dimensions Network for Speaker Recognition,” in *Interspeech 2024*, 2024, pp. 3235–3239.